In Vivo Systems Analysis Identifies Spatial and Temporal Aspects of the Modulation of TNF-α-Induced Apoptosis and Proliferation by MAPKs

Ken S. Lau[1,2,3], **Alwin M. Juchheim**[1,2], **Kimberly R. Cavaliere**[1], **Sarah R. Philips**[1], **Douglas A. Lauffenburger**[3], and **Kevin M. Haigis**[1,2,*]

[1]Molecular Pathology Unit, Center for Cancer Research, and Center for Systems Biology, Massachusetts General Hospital, Charlestown, MA 02129, USA.

[2]Department of Pathology, Harvard Medical School, Boston, MA 02115, USA.

[3]Department of Biological Engineering and Koch Institute for Integrative Cancer Research, Massachusetts Institute of Technology, Cambridge, MA 02139, USA.

Abstract

Cellular responses to external stimuli depend on dynamic features of multi-pathway network signaling; thus, the behavior is of a cell is influenced in a complex manner by its environment and by intrinsic properties. Methods of multi-variate systems analysis have provided an understanding of these convoluted effects, but to date this has been only for relatively simplified in vitro cell culture examples. An unaddressed question is whether such approaches can be successfully brought to bear on in vivo conditions. We have analyzed the in vivo signaling network that determines the response of intestinal epithelial cells to the pro-inflammatory cytokine tumor necrosis factor α (TNF-α). We built data-driven, partial least-squares discriminant analysis (PLSDA) models based on signaling, apoptotic, and proliferative responses in the mouse small intestinal epithelium after systemic exposure to TNF-α. We identified the extracellular signal–regulated kinase (ERK) signaling axis as a critical modulator of the temporal variation in apoptosis at different doses of TNF-α, as well as the spatial variation in proliferative responses in distinct intestinal regions. Pharmacologic inhibition of MEK, a mitogen-activated protein kinase kinase upstream of ERK, integrally altered the signaling network and changed the temporal and spatial phenotypes in accordance with a priori model predictions. Our results demonstrate the dynamic, adaptive nature of in vivo signaling networks and identify natural, tissue-level variation in response phenotypes that can be deconvoluted only with quantitative, multi-variate computational modeling. To our knowledge, this is the first study to apply computational

*To whom correspondence should be addressed. khaigis@partners.org.

modeling of signaling networks to a bona fide in vivo system, and it lays a foundation for the use of systems-based approaches to understand how dysregulation of the cellular network state underlies complex disease.

INTRODUCTION

Inflammation is a critical physiological process in which the body mounts a response to infection or injury by mobilizing hematopoetic cells to the afflicted area to promote tissue repair. Under conditions of recurrent infection or autoimmunity, inflammation can become chronic and debilitating. A prime example of chronic inflammation is inflammatory bowel disease (IBD), an autoimmune disorder that affects approximately 0.4% of the population worldwide (1). A major component of the pathology of IBD is the disruption of normal intestinal epithelial homeostasis, which is presumably elicited by cytokines that are produced by the invading inflammatory cells (2). Because of the central role of intestinal epithelial proliferation and apoptosis in maintaining normal intestinal epithelial homeostasis, it is important to understand how these functional behaviors become dysregulated by exposure to inflammatory cytokines.

Tumor necrosis factor α (TNF-α) is an inflammatory cytokine that activates both pro-death and pro-survival pathways downstream of two receptors, TNFR1 and TNFR2 (3). Dysregulation of TNF-α drives chronic inflammation in humans and mice and antibody-based therapy against TNF-α is used clinically to treat IBD (4–6). The cellular responses that result from engagement of TNFR1 and TNFR2 by TNF-α are varied and complex, as evidenced by conflicting reports of the functions of both receptors. In neurons and cardiomyocytes, TNFR1 is involved in cell death, but TNFR2 plays a protective role (7–11). In the intestinal epithelium, both TNFR1 and TNFR2 are thought to be pro-death (12), whereas other studies have reported that TNFR1 is pro-survival in this tissue (13). Clearly, the phenotypic responses induced by TNF-α are highly context-dependent. Although the molecular pathways that operate downstream of TNFR1 and TNFR2 have been carefully delineated, the network level interactions across multiple pathways that affect phenotypic responses to TNF-α remain largely unknown.

Studies have shown that the regulation of TNF-α-induced apoptosis of epithelial cells involves quantitative integration of multiple signaling pathways downstream of the activation of TNFRs (14, 15), but these investigations were performed in vitro, and subsequent studies have shown that the in vitro cellular response to TNF-α is highly sensitive to the cellular genotype (16). Indeed, it remains unclear whether the TNF-α molecular machinery deciphered in vitro, primarily in transformed cell lines, operates in vivo. Moving the integrative systems analysis approach into an in vivo setting, and into a disease-relevant context, has heretofore remained a major challenge. Here, we have used systems biology to analyze the response of the intestinal epithelium to systemic TNF-α. Because our study was performed entirely in vivo, we have characterized the molecular and cellular responses of wild-type epithelial cells to TNF-α in their natural physiological context.

RESULTS

TNF-α elicits distinct phenotypic responses in different regions of the small intestine

To begin to understand the epithelial response to inflammatory cytokines, we measured the acute apoptotic and proliferative responses of the mouse intestinal epithelium to systemic TNF-α. We initially chose to treat animals with a single bolus of 5 μg of recombinant mouse TNF-α based both on published studies of the physiological effects of exogenous TNF-α in

mice and on preliminary studies performed in our laboratory to assess the magnitude of the induction of apoptosis in the intestinal epithelium by various doses of TNF-α (17, 18). This dose (5 μg) of recombinant cytokine produces a transient spike in the amount of TNF-α in the tissue that is approximately five-fold higher than the basal amount in the intestine and three-fold higher than the amount of tissue TNF-α in a genetic model of inflammatory bowel disease (19). Here, we found that the responses to systemic TNF-α were qualitatively variable along the longitudinal length of the small intestine. The magnitude of TNF-α-induced apoptosis decreased from the duodenum to the ileum, as observed by immunohistochemical analysis of cleaved caspase 3, whereas the reverse was true for proliferation, as assessed by immunohistochemical analysis of phosphorylated histone H3 (Fig. 1A and fig. S1).

We speculated that the variation in phenotypes among the different regions of the intestine might have been because we measured apoptotic and proliferative responses at single time points. To explore the phenotypic variation in more detail, we designed an experiment that could quantitatively measure the phenotypic responses to TNF-α in the different regions of the small intestine in a dynamic fashion (Fig. 1B). A time course revealed that the ileum was intrinsically resistant to TNF-α-induced apoptosis, but that the kinetics of cell death induction in the duodenum were dose-dependent (Fig. 1C). Whereas the apoptotic response in the duodenum gradually peaked at 4 hours after systemic treatment with 5 μg of TNF-α, apoptosis was abruptly induced earlier (peaking at 2 hours) after treatment with a higher dose (10 μg) of TNF-α. Coincident with TNF-α-induced apoptosis in the duodenum, proliferation was largely suppressed in this region early after TNF-α treatment (Fig. 1D). Early proliferative arrest was not observed in the ileum (Fig. 1D).

We next explored whether the initial cellular sensing of the extracellular TNF-α signal might account for the different phenotypes observed in the duodenum and ileum. Indeed, the differential abundance of TNFR1, as assessed by quantitative Western blotting analysis, correlated with the apoptotic phenotypes of the duodenum and ileum (fig. S2A). Immunohistochemical analysis of TNFR1 revealed that the differences in the overall amounts of receptor protein that were detected by Western blotting were not due simply to a quantitative reduction in its abundance, but also involved a substantial restriction of its expression pattern within the villus of the ileum (fig. S2A). In contrast, the abundance of TNFR2 appeared to be consistent between the different intestinal regions (fig. S2B). Nevertheless, although the amount of TNFR1 was substantially reduced in the ileum relative to that in the duodenum, analysis of TNFR1-null animals demonstrated that TNF-α-induced signaling required TNFR1, regardless of the region (fig. S2C). Loss of TNFR2 partially abrogated TNF-α-induced activation of some, but not all, signals in both regions (fig. S2C). Thus, there was no simple correlation between the amounts of TNFR1 and TNFR2 and the phenotypic effects of TNF-α in the duodenum and ileum.

Large-scale signaling data can be collected from an in vivo system

Given the seemingly complex relationship between the abundances of the TNFRs and the phenotypic response to TNF-α, we surmised that taking a network view of the regional, temporal, and dose-dependent differences in the downstream signaling network might shed light on the pathways that modulate TNF-α responses in the intestinal epithelium. To this end, we analyzed signaling in lysates prepared from intestinal samples corresponding to the time course and locations specified in the experimental scheme (Fig. 1B). In total, we created a cue-signal-response dataset that included 3,080 data points (55 mice, 2 regions per mouse, 14 signals per sample, in technical duplicates) composed of phosphorylated proteins that represent critical nodes in various signaling pathways (Fig. 2 and fig. S3). Concentrations of phosphorylated proteins were measured with a Luminex-based capture method, which measures the relative amounts of phosphorylated protein over a large linear

range. As might be expected from an in vivo experiment, there was inter-animal variability in the dataset. The dynamics of signaling were also highly variable between some phosphorylated proteins, and we also observed region- and dose-dependent differences in signaling amplitude and dynamics (fig. S4).

Quantitative Western blotting analysis indicated that, for the majority of the proteins assayed, the differences in TNF-α signaling between the duodenum and ileum could not be explained by differences in the total amounts of a given signaling protein (fig. S5A). Two notable exceptions were c-Jun and Atf2, which were more abundant in the duodenum than in the ileum, and whose phosphorylated forms were increased in abundance in the duodenum after exposure to TNF-α (figs. S4 and S5A). In addition to Western blotting, we used immunohistochemistry to determine the localization of TNF-α-induced protein phosphorylation within the intestine. This analysis demonstrated that signal activation was localized to the intestinal epithelium and not to cells resident in the underlying mesenchyme (fig. S5B).

Partial least squares discriminant analysis (PLSDA) modeling deconvolutes complex in vivo signaling data

To delineate the variation that existed within our signaling dataset, we performed hierarchical clustering of the signaling data, which successfully separated the dataset by region (duodenum versus ileum, Fig. 2). Nevertheless, representation of the dataset in the full signaling space prevented our identification of the underlying signals that contributed to the separation of data, as exemplified by the uninformative clustering of the signals themselves. Moreover, when we performed principal component analysis (PCA) of the signaling dataset we could cluster the data by time in an unsupervised manner (fig. S6A), demonstrating that the data contained biologically meaningful variation.

To develop a predictive classification model that described the temporal variation in TNF-α-induced apoptosis and the spatial variation in proliferation, we used a PCA-based approach called partial least squares discriminant analysis (PLSDA). The principle behind a PLSDA is twofold: (1) the compression of complex multi-dimensional independent variable space into simpler lower dimensional latent variable (LV) space based on covariance and (2) the statistical correlation of independent variables to dependent variables. The advantage of PLS methods is that a quantitative and predictive model can be constructed using only a few latent variables instead of many variables, making it easier to interpret. The latent variables themselves are vector projections of individual phospho-protein signals, termed "loadings," while the dependent variable projections onto latent variable space are called scores (20). We classified the cellular phenotypes into three groups—(i) late apoptosis and arrest, (ii) early apoptosis and arrest, and (iii) no apoptosis and proliferation—and used the signaling time courses as a whole for classification. We selected a two-LV PLSDA model based on the lowest classification error of calibration and cross validation (fig. S6, B to D). The model distinctly classified the scores, with LV 1 accounting for regional variability (the presence or absence of proliferative arrest) in the small intestine, whereas LV 2 described temporal variability in the duodenum (early or late apoptotic peak) (Fig. 3A). With respect to the signals that constitute the LVs, phosphorylation of ATF2 and c-JUN correlated with apoptosis or growth arrest in the duodenum (Fig. 3B). Significant regional- or dose-dependent differences were observed if these signaling time courses were considered individually (Fig. 3C). Late phosphorylation of extracellular signal–regulated kinase ERK, MEK, and RSK correlated with the early apoptotic peak in the duodenum, but transient phosphorylation of ERK, MEK, and P38 mitogen-activated protein kinase correlated with resistance to proliferative arrest in the ileum (Fig. 3B). This result suggests that two separate waves of MAPK activation occurred in response to TNF-α in the intestinal epithelium, with different functional roles and contexts. The early peak occurred only in the ileum and might

be responsible for the maintenance of proliferation following exposure to TNF-α. Early activation of MEK and ERK was substantially reduced in the duodenum, which presumably led to proliferative arrest, which occurred concurrently with TNF-α-induced apoptosis. Under conditions of higher dose (10 μg) of TNF-α in the duodenum, we observed an earlier and more transient cell death response, as opposed to the more gentle and later response to low-dose TNF-α. In this case, we speculated that increased MEK-ERK-RSK signaling was required to maintain homeostasis in the context of a stronger cell death signal, and that this was achieved by sustaining cell survival mechanisms for a longer period of time through a secondary signaling peak. Based on this reasoning, we hypothesized that pharmacologic perturbation of the MAPK signaling axis might alter the apoptotic and proliferative responses of the small intestinal epithelium to systemic TNF-α in a temporally and spatially differential manner.

Inhibition of MEK differentially affects TNF-α-induced apoptosis and proliferation

To test this hypothesis, we treated animals with PD325901, a potent and selective inhibitor of MEK (21), for two hours before systemic injection with TNF-α (5 μg). From these animals (and the corresponding vehicle-treated control mice), we collected a second signaling dataset that consisted of 1,680 data points (30 animals, 2 regions per animal, 14 signals per sample, in technical duplicates) (fig. S7). With our PLSDA model, we applied these signaling data to the derived mathematical function to predict the ultimate phenotypic effect of the inhibition of MEK on TNF-α-induced apoptosis and proliferation in the small intestine. Instead of becoming classified into class 1, similar to the duodenal samples that were treated with 5 μg of TNF-α alone (fig. S8A), the MEK-inhibited duodenal samples were classified into class 2, similar to duodenal samples treated with 10 μg of TNF-α alone (Fig. 4A). As expected, these samples did not classify into class 3, which consists of ileal samples (fig. S8B).

This result can be represented by a shift of the samples along LV2 from the lower left quadrant into the upper left quadrant in our scores plot, predicting that the inhibition of MEK would alter the TNF-α-induced apoptotic response by shifting the apoptotic peak from late to early (Fig. 4B). Note that the MEK-inhibited samples shifted within the distribution of the original model, confirming that the two datasets maintain common network-level relationships between signals and responses, conceptually consistent with previous in vitro findings (14, 15). We verified that the inhibition of MEK suppressed the phosphorylation of ERK while increasing the extent of phosphorylation of MEK itself (fig. S8, C and D), and we then experimentally confirmed our prediction. The apoptotic time course of MEK-inhibited duodenal samples was shifted to an earlier profile, consistent with samples treated with 10 μg of TNF-α (Fig. 4C). This analysis demonstrates the ability of our model to predict the temporal variation in apoptosis in the duodenum.

To predict the effect of modulation of MEK and ERK on proliferation in the small intestine, we first performed PLSDA on our new dataset to examine signaling relationships after MEK inhibition (fig. S9A). The status of c-JUN and ATF2 remained unchanged after MEK inhibition, again correlating positively with the duodenum and negatively with the ileum (fig. S9B). As further support for the association of c-JUN and ATF2 with the duodenum, we found that this pathway was activated during TNF-α-induced apoptosis, a process that does not occur in the ileum (22–24). Because c-JUN and ATF2 could always be used to distinguish the duodenum from the ileum, we omitted them from our subsequent prediction to examine the effect of MEK inhibition on the spatial variation in proliferation in the intestine. As a control, we entered the ileal samples from our calibration dataset, without c-JUN and ATF2, into our predictive model. Removing c-JUN and ATF2 was not sufficient to shift the samples away from class 3 (no apoptosis and proliferation), which consists of ileal samples (fig. S9C). We then applied the ileal portion of our MEK-inhibited signaling dataset

to our model with the same criterion. MEK-inhibited ileal samples now classified into both class 1 (Fig. 5A), similar to the duodenum treated with 5 μg of TNF-α, and into class 3 (fig. S9D). This result was also represented by a partial shift of our samples from the right side to the left side along LV1 in our scores plot, predicting that inhibition of MEK would sensitize the ileum to TNF-α-induced arrest of proliferation (Fig. 5B). Our experimental results validated our prediction, such that MEK inhibition caused partial proliferative arrest in the ileum in response to systemic treatment with 5 μg of TNF-α (Fig. 5C), demonstrating the ability of our model to describe the spatial variation in the regulation of proliferation.

Inhibition of MEK broadly affects the cellular network in a multi-pathway manner

Our global signaling datasets also enabled us to assess whether the molecular effects of MEK inhibition were restricted to the MAPK pathway, or whether there were widespread signaling changes throughout the network. We applied PLSDA to duodenal samples treated with 5 μg of TNF-α that were also treated with PD325901 (Fig. 6A). As expected, transient ERK and RSK activation were anti-correlative with MEK inhibition, confirming that these kinases were downstream of MEK in this context (Fig. 6B). A host of late phosphorylation events were increased under conditions of MEK inhibition, similar to the late activation of the MEK-ERK-RSK pathway in duodenal tissues treated with 10 μg of TNF-α alone. Among these signals were AKT, S6, and, unexpectedly, RSK, which we assume was activated through a MEK-ERK-independent pathway in the presence of PD325901 (Fig. 6C). These results suggest that, in the absence of their primary, pro-survival response to TNF-α (that is, MEK-ERK signaling), intestinal epithelial cells can divert the pro-survival signal through an alternate parallel pathway (that is, through AKT and S6).

We then examined the predictive ability of our model without systems-level, multivariate information; that is, by assuming that a perturbation would affect only a single pathway. To test MEK inhibition in this context, we set the level of ERK phosphorylation to zero in our calibration dataset without changing any other values, and then applied this dataset to our predictive model. In contrast to the experimental dataset, the duodenal samples from this artificial MEK-inhibited dataset remained in the lower left quadrant (Fig. 7A). This uni-variate approach thus generated a prediction that the phenotypic response would not change after inhibition of MEK, which was contrary to the experimental data. The ileal samples shifted to the left along LV1, similar to the experimental MEK-inhibited dataset, supporting a phenotypic change dominated by the single pathway modulation (Fig. 7B). Together, these results demonstrate that a multivariate systems approach is needed to understand the integrated operation of some biological pathways and phenomena, whereas a single-pathway, reductionist approach is sufficient to understand others.

DISCUSSION

TNF-α is a pleiotropic signaling molecule that induces both pro-death and pro-survival signals under different circumstances. Physiologically, TNF-α is a critical regulator of inflammatory responses, but the phenotypic effects of inflammatory TNF-α on specific organs are context-dependent. As such, it is critical to study the biological effects of this inflammatory cytokine in the natural tissue environment. In this study, we evaluated the response of the mouse small intestinal epithelium to TNF-α, which drives the onset and progression of IBD. Even within this singular organ, the epithelial response to TNF-α was highly dependent upon regional context (Fig. 1A). In the duodenum, TNF-α strongly induced apoptosis, the timing of which was dependent upon the amount of circulating TNF-α (Fig. 1C). In the ileum, TNF-α did not induce apoptosis, but instead induced proliferation (Fig. 1D). This natural physiological variation formed the foundation for our efforts to use quantitative computational modeling to integrate TNF-α-induced signaling with overall

cellular response in vivo. Our model implicated ERK signaling in both the temporal and spatial phenotypic variations associated with TNF-α in this system.

The ERK pathway is primarily known as a mitogenic pathway that induces proliferation upon growth factor stimulation, but it also performs a constellation of other functions. ERK is multifunctional by virtue of its two structurally distinct substrate-docking sites. The docking site for ERK, FXFP (DEF)-domain regulates the phosphorylation and activation of nuclear transcription factors, such as ELK-1, that control proliferation, whereas the D-domain regulates the activation of cytoplasmic targets, such as RSK (25). RAK acts downstream of the ERK pathway to promote cell survival (26). As with TNF-α, however, the survival function of ERK is highly context-dependent. Whereas ERK signaling is typically associated with enhanced survival, ERK promotes cell death in response to interferon-γ (IFN-γ) by phosphorylating death-associated protein kinase (DAPK), which, like RSK, binds to ERK through a D-domain (27).

Evidently, the context in which ERK is activated determines the functional outcome. In this study, we discovered that the temporal and regional context of ERK activation was indicative of the phenotypic outcome. We observed two different patterns of ERK activation by TNF-α, an early phase in the ileum and a late phase in the duodenum. The early activation of ERK in the ileum was likely due to the direct activation of the pathway by TNF-α (28–32). Based on our computational model, we hypothesized that early ERK signaling in the ileum was important for maintaining a basal extent of proliferation in the presence of TNF-α. Indeed, when we inhibited MEK pharmacologically, TNF-α suppressed cellular proliferation in the ileum, just as it did in the duodenum (Fig. 5C). Note that this proliferative phenotype was not directly connected to apoptosis, as evidenced by the inability of TNF-α to induce apoptosis in the ileum in the context of MEK inhibition. Moreover, the timing of the ERK effect on proliferation (30 min after treatment with TNF-α) indicated that it was not a compensatory mechanism to account for the widespread apoptosis that occurred 2 to 4 hours after exposure to TNF-α, but rather a direct effect of TNF-α on cellular proliferative pathways. Thus, in this context, ERK activation in the presence of TNF-α enabled the intestinal epithelium to maintain its normally high proliferative index. TNF-α-induced hyperproliferation occurred in the ileum 2 to 4 hours after treatment, but this phenotype appeared to be largely ERK-independent (Fig. 5C).

The duodenum differed from the ileum with respect to its cellular response to TNF-α and also in the kinetics of ERK activation after exposure. Early apoptosis (2 hours after treatment with 10 μg of TNF-α) was associated with a secondary ERK activation 4 hours after exposure (fig. S4). Judging from the relationship between the apoptotic peak at 2 hours after TNF-α treatment and ERK signaling at 4 hours, ERK signaling in the duodenum, although correlative with apoptosis, was probably not causal. Instead, it likely reflected the adjustment of the signaling network to adapt to a new phenotypic state. Nevertheless, our model predicted that the temporal apoptotic phenotype could be modulated indirectly by perturbing ERK signaling. As predicted, pharmacologic inhibition of MEK shifted the apoptotic time course to an earlier time in animals treated with a low dose of TNF-α (Fig. 4C). The mechanisms underlying the late activation of ERK after exposure to a high dose of TNF-α in the duodenum remain to be elucidated, but may include autocrine or paracrine signals that are released into the microenvironment.

In addition to deciphering the complex role of ERK signaling in TNF-α-induced proliferation and apoptosis in the intestinal epithelium, our study demonstrates the importance of network-level regulation of complex phenotypes, and indicates that models based on local pathway changes will have limited predictive use. Indeed, our results demonstrated that perturbation of a single node (MEK) in the signaling network not only

affected the neighboring nodes (ERK), but also altered the state of the entire network (Fig. 6C). The physiological relevance of this observation is clear in that most diseases result from complex perturbations of the signaling network that are secondary to both environmental and genetic factors. As a result, targeted therapies designed solely to directly inhibit a chronically dysregulated pathway may not have the predicted effects, because the whole network may have adapted to a new signaling state. Indeed, drug-induced perturbations can cause widespread changes in gene expression and signaling in cell lines (33, 34). There are two underlying causes of these network level changes: primary off-target effects of drugs, which can be resolved with more critical design of specific molecules, and pathway feedback or cross-talk, or both, which can only be resolved through deeper understanding and new methods of analysis (35, 36). Given the high specificity of PD325901 for MEK (21), the network-level changes observed in our experiment likely resulted from feedback and cross-talk between the MAPK pathway and the rest of the network.

The discrepancy in the responses of the duodenum and ileum to TNF-α represents a example of how subtle changes in natural physiology can strongly affect phenotypic outcome. These subtle variations that occur in vivo are virtually impossible to study in vitro. In tissues, cells undergo differentiation, interact directly with homologous and heterologous cell types, and receive signals from the extracellular microenvironment. All of these interactions can provide cues that affect the cellular response to perturbation. Measuring a wide range of nodes in the global signaling network provides "surrogate" information that can integrate activities distributed across many pathways (15). Our study demonstrates that enough surrogate information can be captured in our signaling dataset to describe the in vivo context. This surrogate information can be analyzed and understood by multivariate, data-driven models, as applied previously to in vitro cell culture systems. For any biological phenomenon, the transition from an in vitro to in vivo system represents a giant leap in understanding and application. Our study provides a case that demonstrates how network-level signaling information can be used to depict in vivo apoptotic and proliferative phenotypes, and to generate testable hypotheses from model predictions.

Together, our study demonstrates that systems-level approaches can be applied to in vivo systems and will ultimately be useful for understanding complex physiological phenotypes. Indeed, a more thorough understanding of signaling pathway circuitry and, in particular, signaling perturbations in pathological contexts, is critical to developing new therapies.

MATERIALS AND METHODS

Animals, treatments, and tissue isolation

All of the animals used in this study, including TNFR1 and TNFR2 knockout mice, were eight-week-old males on a C57BL/6J genetic background (Jackson Laboratory). In our initial experiment, animals were anesthetized with Avertin (tribromoethanol, 250 mg/kg) and then administered 5 or 10 μg of recombinant mouse TNF-α (Abazyme) in phosphate-buffered saline (PBS, 50 μl total volume) by retro-orbital injection. These mice were sacrificed according to a time course after TNF-α treatment. Control animals were anesthetized, injected with PBS (50 μl) by retro-orbital injection, and then sacrificed two hours later. For the MEK inhibition experiment, animals were anesthetized with Avertin and then treated with PD325901 (12.5 mg/kg, ChemieTek), solubilized with 10% DMSO in PBS, by retro-orbital injection. Two hours later, animals were again anesthetized and treated with TNF-α, as in the original experiment. In this experiment, control animals were pretreated with vehicle two hours prior to TNF-α. After treatment with TNF-α, animals were sacrificed and the small intestine was removed and rinsed in PBS. Duodenal and ileal tissues were lysed and homogenized immediately in Bio-Plex lysis buffer (Bio-Rad), or else

fixed with formalin for subsequent immunohistochemical analysis. Duodenal samples were obtained from the 1 cm of small intestinal immediately adjacent to the stomach. Ileal samples were obtained from the 3 cm of small intestine immediately adjacent to the cecum. All animal work performed in this study was undertaken according to approved protocols and animal welfare regulations as put forth by the Subcommittee on Research Animal Care at the MGH.

Quantification of apoptosis and proliferation

Apoptosis was measured by performing quantitative Western blotting analysis of the amount of cleaved caspase 3 in the same tissue lysates that were used for Bio-Plex signaling analysis. Thus, each region from an individual animal represents a single measurement. Western blots were quantified on a Li-Cor Odyssey infrared imaging system. Proliferation was quantified by immunohistochemistry for the presence of phosphorylated histone H3, using standard methodology. Briefly, tissue sections (5 μm) of duodenum or ileum were screened for crypts that were sectioned longitudinally. In these crypts, the number of cells that contained phosphorylated histone H3 was counted. Because each intestinal crypt is an independent clonal unit, each count represents an individual measurement. In total, approximately 2,300 crypts were counted from the 85 animals in the study.

Bio-Plex signaling analysis

The dataset consisting of quantitative measurements of protein phosphorylation was collected from lysed samples by Bio-Plex (Bio-Rad) with available phospho-signaling assay kits: phosphorylated inhibitor of nuclear factor κβ α (pIκβα, Ser^{32} and Ser^{36}), phosphorylated c-JUN N-terminal kinase (pJNK, Thr^{183} and Tyr^{185}), pMEK1 (Ser^{217} and Ser^{221}), pERK1 (Thr^{202} and Tyr^{204}) and pERK2 (Thr^{185} and Tyr^{187}), pRSK (Thr^{359} and Ser^{363}), pP38 (Thr^{180} and Tyr^{182}), pc-JUN (Ser^{63}), pATF2 (Thr^{71}), pAKT (Ser^{473}), pS6 (Ser^{235} and Ser^{236}), phosphorylated signal transducer and activator of transduction 3 (pSTAT3, Ser^{727}), pSTAT3 (Tyr^{705}), and total MEK1. Tissue lysates were quantified by BCA (Pierce), and equal amounts of protein from each sample were used for the Bio-Plex assays: 4 μg of proteins were used for assays of pJNK, pAKT, pSTAT3 (Tyr^{705}), and pATF2, whereas 1.5 μg of proteins were used for the rest of the assays. These protein amounts were determined experimentally to be within the linear ranges of activity of these assays on small intestinal tissue samples prior to this analysis. All protein phosphorylation measurements were normalized to a common control cell line lysate for assays between plates to be comparable. The dataset was also normalized based on the amounts of total MEK, an internal control assay, but the results obtained were not significantly different from those obtained without performing this normalization.

Protein analysis

Quantitative Western blotting analysis was performed with the LiCor Odyssey platform, with antibodies (from Cell Signaling Technologies) against the following proteins: Iκβα, JNK, MEK1,2, ERK1,2, RSK1,2,3, P38, c-JUN, ATF2, AKT, S6, STAT3, and cleaved caspase 3. Antibodies against TNFR1 and TNFR2 were from Santa Cruz Biotechnology. Immunohistochemistry was performed by standard protocols with antibodies from Cell Signaling Technologies for cleaved caspase 3, phosphorylated histone H3, and pc-JUN (Ser^{63}).

Quantitative modeling

Heat maps and hierarchical clustering of the dataset were generated with the Bioinformatics toolbox in Matlab (Mathworks). Statistical models were constructed with Matlab PLS Toolbox 5.5 (Eigenvector), with each replicate mouse treated as an individual sample

instead of the average, so that the model could account for biological variability. Data were normalized by mean-centering and variance-scaling. For PCA modeling, the input matrix was organized such that the samples were combinations of mouse, region, dose, and time to capture protein phosphorylation measurements that covariate together with time. For PLSDA, the input matrix was organized such that all time points of the time courses for all signals were included for each sample (for each combination of mouse, region, and dose). Cross validation was performed with the contiguous block method.

Supplementary Material

Refer to Web version on PubMed Central for supplementary material.

Acknowledgments

REFERENCES AND NOTES

1. Lakatos PL. Recent trends in the epidemiology of inflammatory bowel diseases: up or down? World J. Gastroenterol. 2006; 12:6102–6108. [PubMed: 17036379]

2. Abraham C, Cho JH. Inflammatory bowel disease. New Engl. J. Med. 2009; 361:2066–2078. [PubMed: 19923578]

3. Bradley JR. TNF-mediated inflammatory disease. J. Pathol. 2008; 214:149–160. [PubMed: 18161752]

4. Rutgeerts P, Sandborn WJ, Feagan BG, Reinisch W, Olson A, Johanns J, Travers S, Rachmilewitz D, Hanauer SB, Lichtenstein GR, de Villiers WJ, Present D, Sands BE, Colombel JF. Infliximab for induction and maintenance therapy for ulcerative colitis. New Engl. J. Med. 2005; 353:2462–2476. [PubMed: 16339095]

5. Kontoyiannis D, Pasparakis M, Pizarro TT, Cominelli F, Kollias G. Impaired on/off regulation of TNF biosynthesis in mice lacking TNF AU-rich elements: implications for joint and gut-associated immunopathologies. Immunity. 1999; 10:387–398. [PubMed: 10204494]

6. Popivanova BK, Kitamura K, Wu Y, Kondo T, Kagaya T, Kaneko S, Oshima M, Fujii C, Mukaida N. Blocking TNF-alpha in mice reduces colorectal carcinogenesis associated with chronic colitis. J. Clin. Invest. 2008; 118:560–570. [PubMed: 18219394]

7. Al-Lamki RS, Brookes AP, Wang J, Reid MJ, Parameshwar J, Goddard MJ, Tellides G, Wan T, Min W, Pober JS, Bradley JR. TNF receptors differentially signal and are differentially expressed and regulated in the human heart. Am. J. Transplant. 2009; 9:2679–2696. [PubMed: 19788501]

8. Wang M, Crisostomo PR, Markel TA, Wang Y, Meldrum DR. Mechanisms of sex differences in TNFR2-mediated cardioprotection. Circulation. 2008; 118:S38–S45. [PubMed: 18824767]

9. Flaherty MP, Guo Y, Tiwari S, Rezazadeh A, Hunt G, Sanganalmath SK, Tang XL, Bolli R, Dawn B. The role of TNF-alpha receptors p55 and p75 in acute myocardial ischemia/reperfusion injury and late preconditioning. J. Mol. Cell. Cardiol. 2008; 45:735–741. [PubMed: 18824172]

10. Defer N, Azroyan A, Pecker F, Pavoine C. TNFR1 and TNFR2 signaling interplay in cardiac myocytes. J. Biol. Chem. 2007; 282:35564–35573. [PubMed: 17913704]

11. Marchetti L, Klein M, Schlett K, Pfizenmaier K, Eisel UL. Tumor necrosis factor (TNF)-mediated neuroprotection against glutamate-induced excitotoxicity is enhanced by N-methyl-D-aspartate receptor activation. Essential role of a TNF receptor 2-mediated phosphatidylinositol 3-kinase-dependent NF-kappa B pathway. J. Biol. Chem. 2004; 279:32869–32881. [PubMed: 15155767]

12. Stillie R, Stadnyk AW. Role of TNF receptors, TNFR1 and TNFR2, in dextran sodium sulfate-induced colitis. Inflamm. Bowel Dis. 2009; 15:1515–1525. [PubMed: 19479745]

13. Ebach DR, Newberry R, Stenson WF. Differential role of tumor necrosis factor receptors in TNBS colitis. Inflamm. Bowel Dis. 2005; 11:533–540. [PubMed: 15905700]

14. Janes KA, Albeck JG, Gaudet S, Sorger PK, Lauffenburger DA, Yaffe MB. A systems model of signaling identifies a molecular basis set for cytokine-induced apoptosis. Science. 2005; 310:1646–1653. [PubMed: 16339439]

15. Miller-Jensen K, Janes KA, Brugge JS, Lauffenburger DA. Common effector processing mediates cell-specific responses to stimuli. Nature. 2007; 448:604–608. [PubMed: 17637676]

16. Kreeger PK, Mandhana R, Alford SK, Haigis KM, Lauffenburger DA. RAS mutations affect tumor necrosis factor-induced apoptosis in colon carcinoma cells via ERK-modulatory negative and positive feedback circuits along with non-ERK pathway effects. Cancer Res. 2009; 69:8191–8199. [PubMed: 19789336]

17. Lee EG, Boone DL, Chai S, Libby SL, Chien M, Lodolce JP, Ma A. Failure to regulate TNF-induced NF-kappaB and cell death responses in A20-deficient mice. Science. 2000; 289:2350–2354. [PubMed: 11009421]

18. Yan F, John SK, Wilson G, Jones DS, Washington MK, Polk DB. Kinase suppressor of Ras-1 protects intestinal epithelium from cytokine-mediated apoptosis during inflammation. J. Clin. Invest. 2004; 114:1272–1280. [PubMed: 15520859]

19. Matharu KS, Mizoguchi E, Cotoner CA, Nguyen DD, Mingle B, Iweala OI, McBee ME, Stefka AT, Prioult G, Haigis KM, Bhan AK, Snapper SB, Murakami H, Schauer DB, Reinecker HC, Mizoguchi A, Nagler CR. Toll-like receptor 4-mediated regulation of spontaneous Helicobacter-dependent colitis in IL-10-deficient mice. Gastroenterology. 2009; 137:1380–1390. [PubMed: 19596011]

20. Wold S, Sjostrom M, Eriksson L. PLS-regression: a basic tool of chemometrics. Chemometr. Intell. Lab. 2001; 58:109–130.

21. Bain J, Plater L, Elliott M, Shpiro N, Hastie CJ, McLauchlan H, Klevernic I, Arthur JS, Alessi DR, Cohen P. The selectivity of protein kinase inhibitors: a further update. Biochem. J. 2007; 408:297–315. [PubMed: 17850214]

22. Singh N, Sun Y, Nakamura K, Smith MR, Colburn NH. C-JUN/AP-1 as possible mediators of tumor necrosis factor-alpha-induced apoptotic response in mouse JB6 tumor cells. Oncol. Res. 1995; 7:353–362. [PubMed: 8747598]

23. Haridas V, Darnay BG, Natarajan K, Heller R, Aggarwal BB. Overexpression of the p80 TNF receptor leads to TNF-dependent apoptosis, nuclear factor-kappa B activation, and c-Jun kinase activation. J. Immunol. 1998; 160:3152–3162. [PubMed: 9531270]

24. Roulston A, Reinhard C, Amiri P, Williams LT. Early activation of c-Jun N-terminal kinase and p38 kinase regulate cell survival in response to tumor necrosis factor alpha. J. Biol. Chem. 1998; 273:10232–10239. [PubMed: 9553074]

25. Dimitri CA, Dowdle W, MacKeigan JP, Blenis J, Murphy LO. Spatially separate docking sites on ERK2 regulate distinct signaling events in vivo. Curr. Biol. 2005; 15:1319–1324. [PubMed: 16051177]

26. Shimamura A, Ballif BA, Richards SA, Blenis J. Rsk1 mediates a MEKMAP kinase cell survival signal. Curr. Biol. 2000; 10:127–135. [PubMed: 10679322]

27. Chen CH, Wang WJ, Kuo JC, Tsai HC, Lin JR, Chang ZF, Chen RH. Bidirectional signals transduced by DAPK-ERK interaction promote the apoptotic effect of DAPK. EMBO J. 2005; 24:294–304. [PubMed: 15616583]

28. Yan F, John SK, Polk DB. Kinase suppressor of Ras determines survival of intestinal epithelial cells exposed to tumor necrosis factor. Cancer Res. 2001; 61:8668–8675. [PubMed: 11751383]

29. Dumitru CD, Ceci JD, Tsatsanis C, Kontoyiannis D, Stamatakis K, Lin JH, Patriotis C, Jenkins NA, Copeland NG, Kollias G, Tsichlis PN. TNF-alpha induction by LPS is regulated posttranscriptionally via a Tpl2/ERK-dependent pathway. Cell. 2000; 103:1071–1083. [PubMed: 11163183]

30. Eliopoulos AG, Dumitru CD, Wang CC, Cho J, Tsichlis PN. Induction of COX-2 by LPS in macrophages is regulated by Tpl2-dependent CREB activation signals. EMBO J. 2002; 21:4831–4840. [PubMed: 12234923]

31. Eliopoulos AG, Wang CC, Dumitru CD, Tsichlis PN. Tpl2 transduces CD40 and TNF signals that activate ERK and regulates IgE induction by CD40. EMBO J. 2003; 22:3855–3864. [PubMed: 12881420]

32. Das S, Cho J, Lambertz I, Kelliher MA, Eliopoulos AG, Du K, Tsichlis PN. Tpl2/cot signals activate ERK, JNK, and NF-kappaB in a cell-type and stimulus-specific manner. J. Biol. Chem. 2005; 280:23748–23757. [PubMed: 15833743]

33. Lamb J, Crawford ED, Peck D, Modell JW, Blat IC, Wrobel MJ, Lerner J, Brunet JP, Subramanian A, Ross KN, Reich M, Hieronymus H, Wei G, Armstrong SA, Haggarty SJ, Clemons PA, Wei R, Carr SA, Lander ES, Golub TR. The Connectivity Map: using gene-expression signatures to connect small molecules, genes, and disease. Science. 2006; 313:1929–1935. [PubMed: 17008526]

34. Kumar N, Afeyan R, Kim HD, Lauffenburger DA. Multipathway model enables prediction of kinase inhibitor cross-talk effects on migration of Her2-overexpressing mammary epithelial cells. Mol. Pharmacol. 2008; 73:1668–1678. [PubMed: 18349105]

35. Fabian MA, Biggs WH 3rd, Treiber DK, Atteridge CE, Azimioara MD, Benedetti MG, Carter TA, Ciceri P, Edeen PT, Floyd M, Ford JM, Galvin M, Gerlach JL, Grotzfeld RM, Herrgard S, Insko DE, Insko MA, Lai AG, Lelias JM, Mehta SA, Milanov ZV, Velasco AM, Wodicka LM, Patel HK, Zarrinkar PP, Lockhart DJ. A small molecule-kinase interaction map for clinical kinase inhibitors. Nat. Biotechnol. 2005; 23:329–336. [PubMed: 15711537]

36. Natarajan M, Lin KM, Hsueh RC, Sternweis PC, Ranganathan R. A global analysis of cross-talk in a mammalian cellular signalling network. Nat. Cell Biol. 2006; 8:571–580. [PubMed: 16699502]
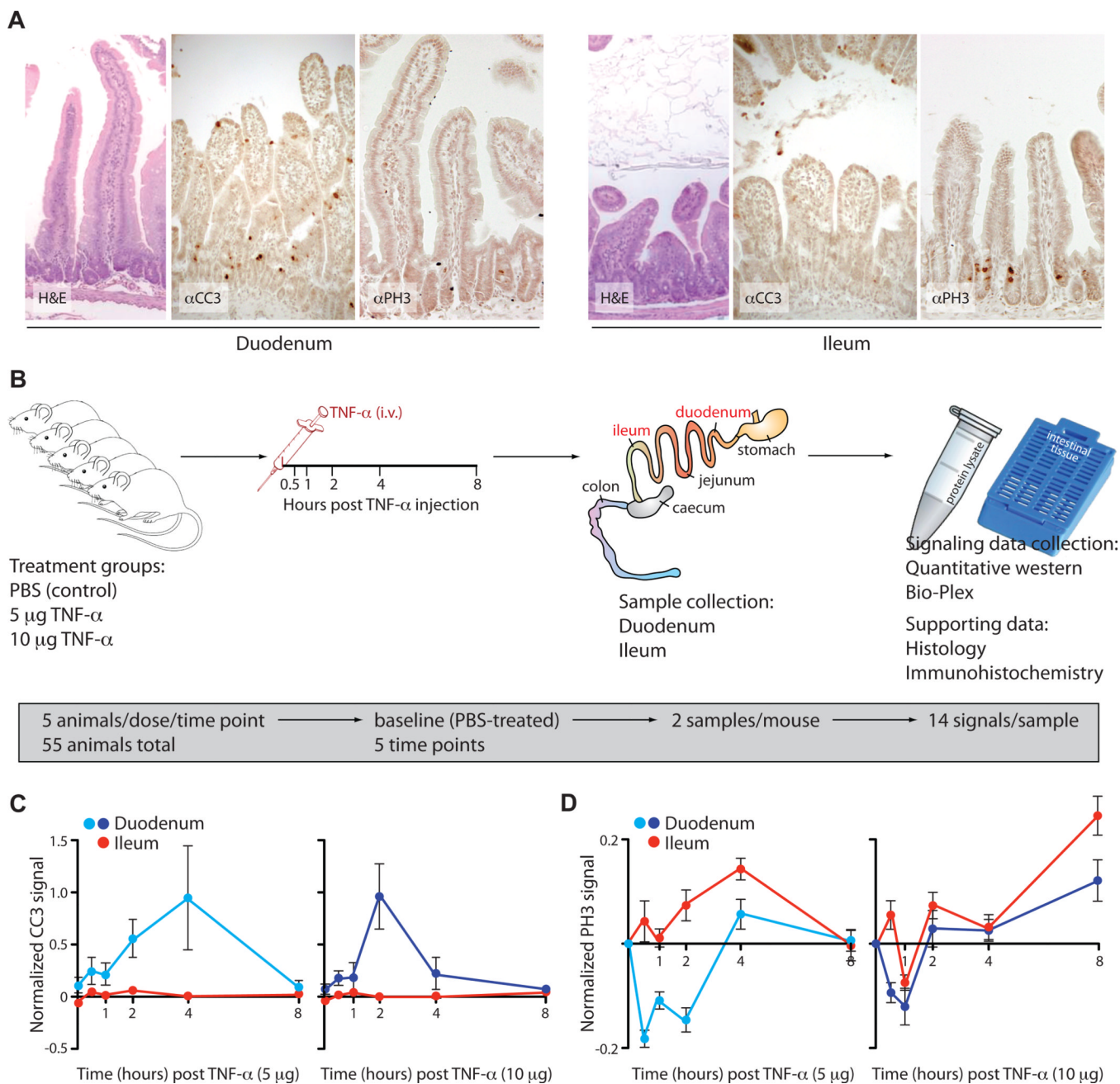
Fig. 1.
Regional dependence of the apoptotic and proliferative responses to TNF-α in the mouse small intestinal epithelium. (**A**) Morphological heterogeneity across the regions of the small intestine, as represented by H&E staining. The apoptotic response to TNF-α, as assessed by immunohistochemical analysis of cleaved caspase 3 (αCC3) at 4 hours after treatment with TNF-α (5 μg), and the proliferative response, as assessed by immunohistochemical analysis of phosphorylated histone H3 (αPH3) 30 min after treatment with TNF-α (5 μg), of the intestinal epithelium varies by region. (**B**) Schematic representation of the experimental design. After injection of mice with TNF-α (5 or 10 μg in PBS), protein lysates and tissue samples were obtained from the duodenum and ileum. In addition to 5 control animals that were mock-treated with PBS, 5 mice were analyzed for each dose of TNF-α at each time

point (from 30 min to 8 hours). The Bio-Plex platform was used to generate phospho-protein signaling data, whereas quantitative Western blotting analysis was used to quantify apoptosis and total protein abundance. Immunohistochemical analysis was used to determine the localization of signals and to quantify the number of proliferating cells. (**C**) Time-course of apoptotic responses in the duodenum and ileum, as determined by quantitative Western blotting for CC3. Error bars represent the standard error of the mean (SEM) from five independent experiments. (**D**) Time-course of proliferative responses in the duodenum and ileum, as determined by enumerating the number of PH3-positive cells per crypt. Error bars represent the SEM from the numbers of crypts counted.

Fig. 2.
Time- and region-dependent signaling datasets in response to TNF-α. Hierarchical clustering of phosphorylated proteins measured by Bio-Plex. The intensity of the green color represents the average of technical duplicates of the median fluorescent intensity (normalized to the highest value of each signal) resulting from each assay. Regional and treatment groupings are signified by color at the top of the heat map. Data are compiled from five independent experiments. Phosphorylated protein signals corresponding to each row are listed on the right side of the heat map.
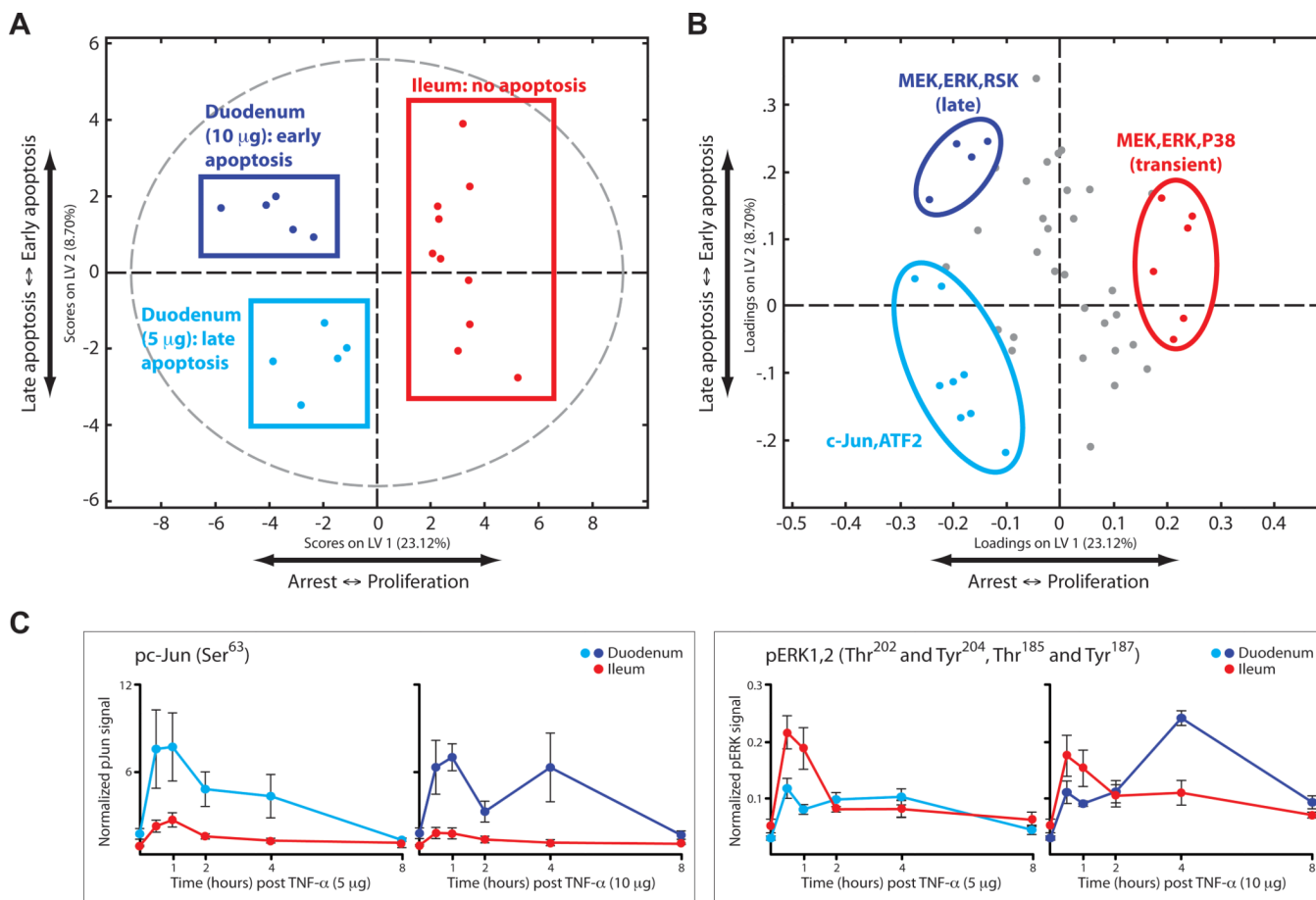
Fig. 3.
Statistical modeling of the in vivo signaling network describes the temporal and spatial variation in TNF-α-dependent phenotypes. (**A**) A PLSDA model constructed from the signaling dataset correlated with apoptosis and proliferation. Scores generated by the model. The dotted gray line represents the 95% confidence limit of the distribution of the scores. Three diverse phenotypic classes are delineated: late apoptosis and arrest (duodenum + 5 μg TNF-α, in cyan), early apoptosis and arrest (duodenum + 10 μg TNF-α, in blue), and no apoptosis or proliferation (ileum, in red). The percentages on the x-and y-axes represent the percentage of variance in the data set captured in a particular LV. (**B**) Loadings generated by the PLSDA model. Signals that contribute most to each phenotypic classification are labeled accordingly with the corresponding color scheme. (**C**) Representative signaling time courses for signals that distinguish between the classes, pc-JUN and pERK, from Bio-Plex analysis. Error bars represent the SEM from five independent experiments.
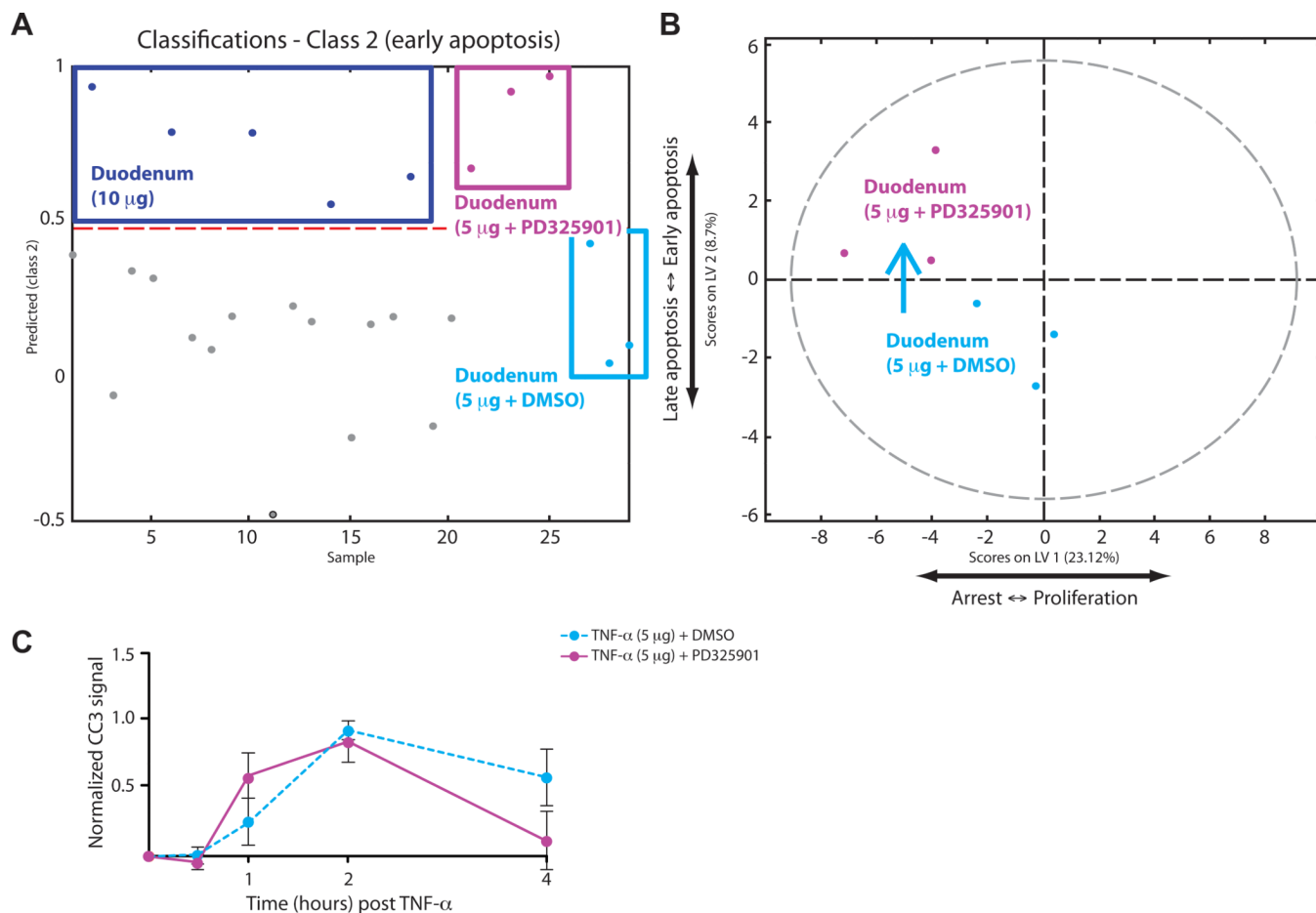
Fig. 4.
Model prediction and experimental test of the effect of MEK inhibition on TNF-α-induced apoptosis in the duodenum. (**A**) PLSDA model–based prediction of the apoptotic phenotype in the duodenum using phosphorylated protein abundance data from samples derived from animals treated with of TNF-α (5 μg) after pre-treatment with PD325901 (purple) or vehicle (10% DMSO in PBS, cyan), relative to samples from animals treated with 10 μg of TNF-α (blue). The y-axis shows the numerical result calculated with the PLSDA function of classification into the "early apoptosis" (class 2) phenotypic class. The red broken line is the threshold defining classification. (**B**) Scores plotted onto the LV1 and LV2 space of the PLSDA model showing the translocation of duodenal samples treated with TNF-α (5 μg) from the lower-left to the upper-left quadrant after MEK inhibition. (**C**) Experimental time-course of apoptosis induced in the duodenum by TNF-α (5 μg) after pretreatment with PD325901 (solid purple line) or vehicle (dotted cyan line). Error bars represent the SEM from three independent experiments.
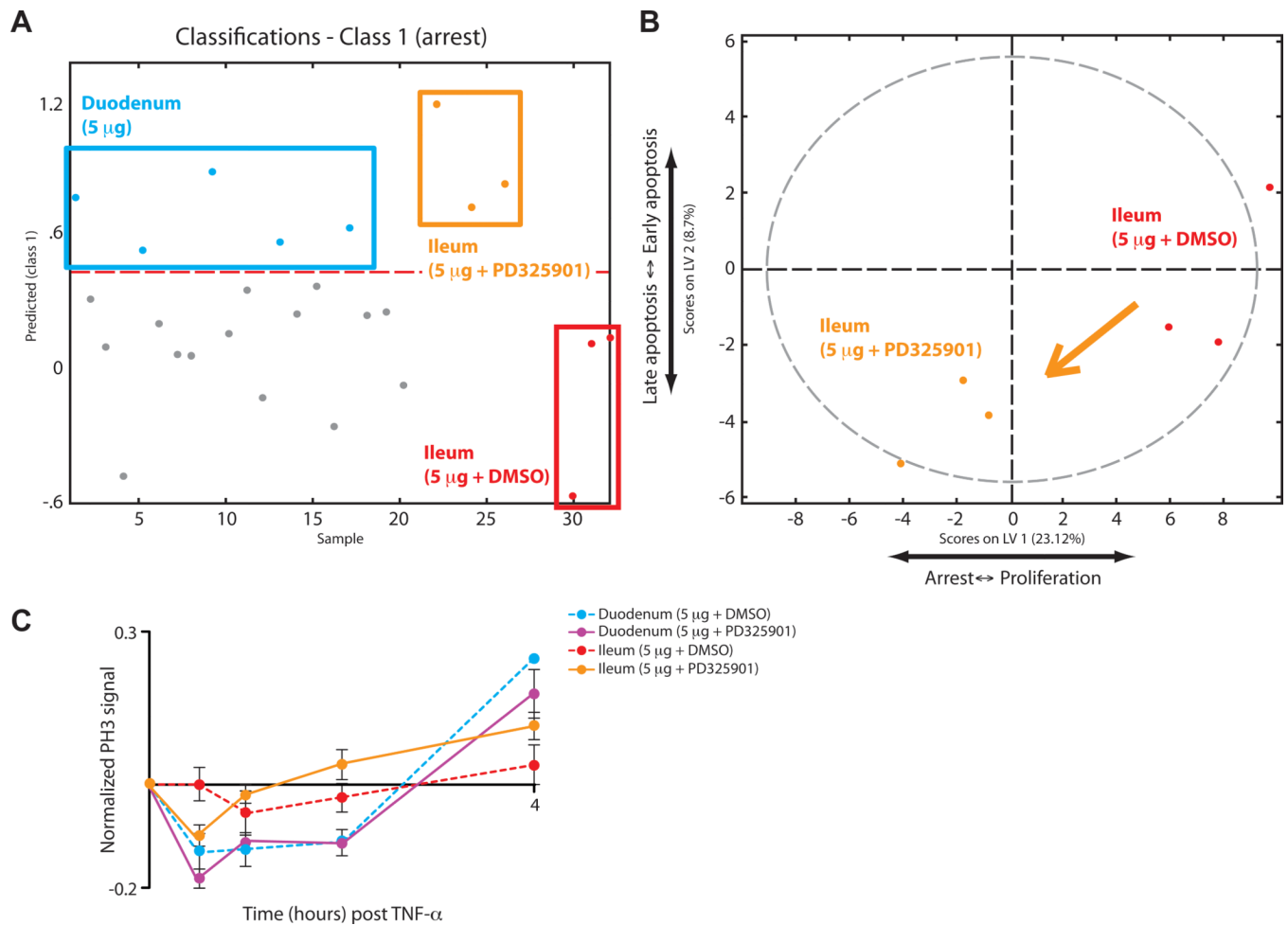
Fig. 5.
Model prediction and experimental test of the effect of MEK inhibition on TNF-α-induced proliferation in the ileum. (**A**) PLSDA model–based prediction of the classification into the "arrest" (class 1) phenotypic class using signaling data of ileal samples from mice treated with TNF-α (5 μg) after pre-treatment with PD325901 (orange) or vehicle (10% DMSO in PBS, red), relative to duodenal samples from mice treated with TNF-α (5 μg, cyan). (**B**) Scores plotted onto the LV1 and LV2 space of the PLSDA model showing the partial translocation of ileal samples treated with TNF-α-(5 μg) from the right half to the left half after inhibition of MEK. (**C**) Experimental time-course of proliferation induced by TNF-α (5 μg) in the duodenum and ileum after pretreatment with PD325901 (solid lines) or vehicle (dotted lines). Error bars represent the SEM from three independent experiments.
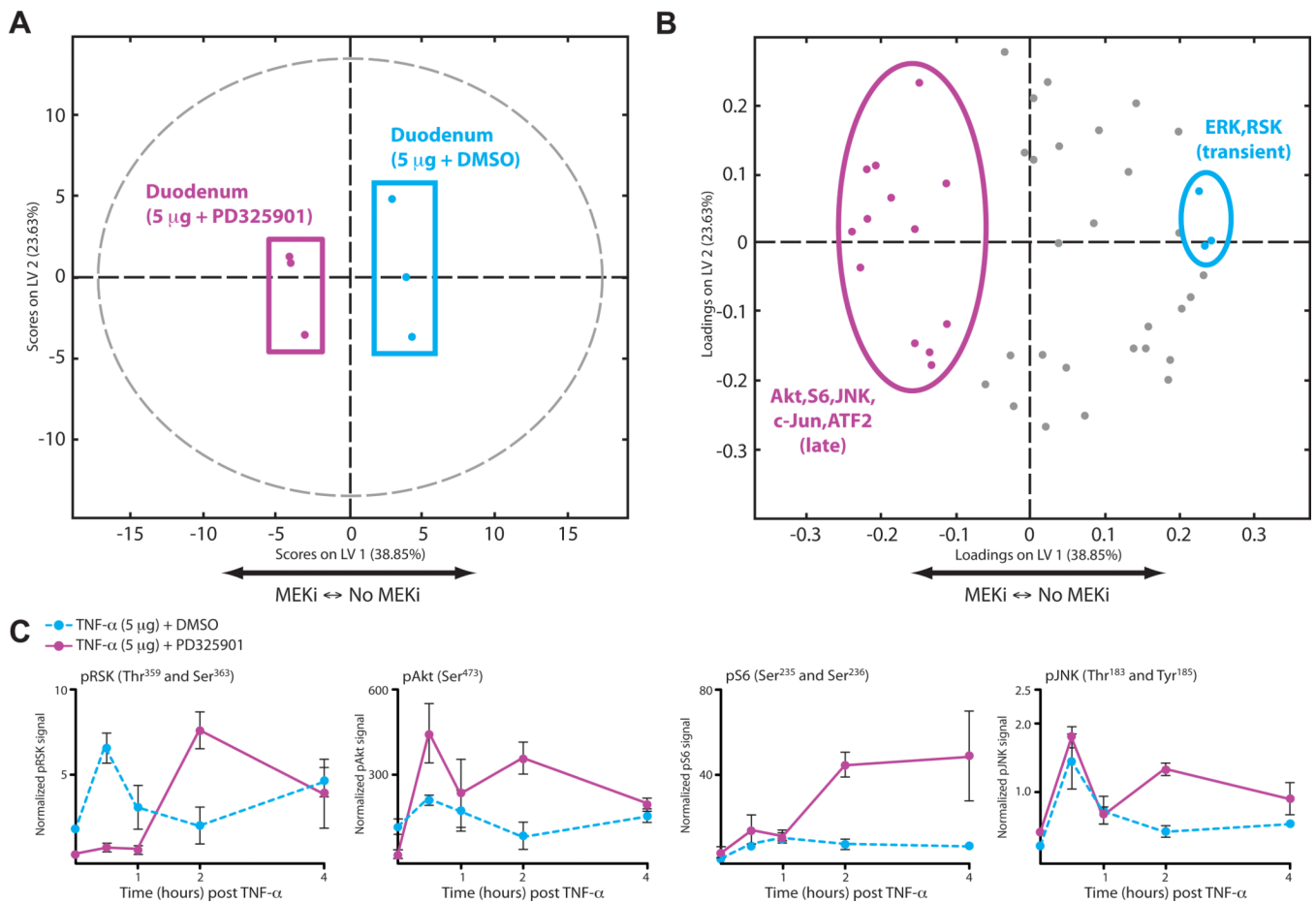
Fig. 6.
Inhibition of MEK initiates a global change in the TNF-α signaling network. (**A**) Scores of a 1D PLSDA model that separate TNF-α treatment (5 μg) in the duodenum with MEK inhibition (purple) from that with DMSO (cyan). The model is plotted in two dimensions for visual purposes. (**B**) Loadings of the model in (A). Signals that contribute most to each classification are labeled accordingly in the corresponding color scheme. (**C**) Abundances of specific phosphorylated proteins that most strongly distinguish the TNF-α-dependent phenotypes between the duodenal samples that were treated with PD325901 (solid purple line) from those that were treated with vehicle (dotted cyan line). Error bars represent the SEM from three independent experiments.
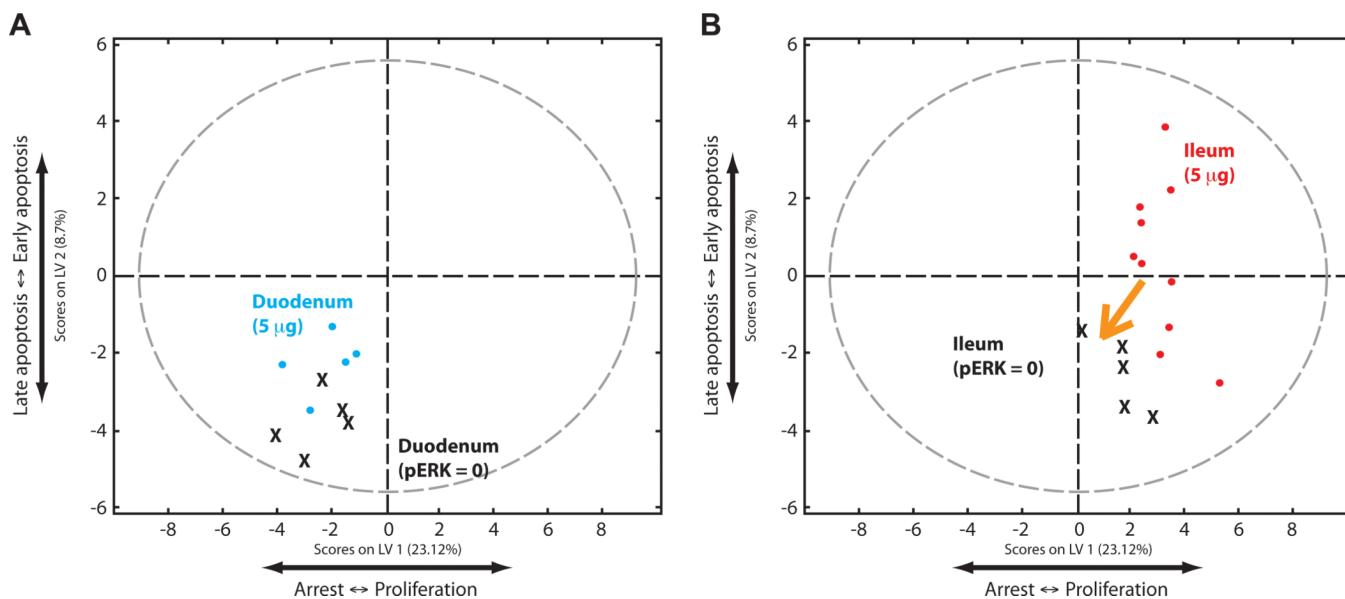
Fig. 7.
The effect of local changes in the signaling network by inhibiting MEK. (**A**) PLSDA scores plot of an artificial duodenal dataset generated by setting the level of pERK to 0 in individual samples while leaving all other values the same (denoted as X on the plot). This dataset was compared to the original calibration dataset (cyan). Note that the artificial dataset does not shift. (**B**) PLSDA scores plot of an artificial dataset generated by setting the ratio of pMEK to pERK to 0, while leaving all other values the same, in ileal samples (X) of the calibration dataset, relative to the ileal samples of the original calibration dataset (red). Note that the artificial dataset shifts partially to the left.